Calculation of F−19 NMR chemical shifts in uranium complexes using density functional theory and pseudopotentials

ARTICLE *in* CHEMICAL PHYSICS · APRIL 2005

Impact Factor: 1.65 · DOI: 10.1016/J.Chemphys.2004.10.041

Available online at www.sciencedirect.com
SCIENCE DIRECT®
Chemical Physics 311 (2005) 45–56
Chemical Physics
www.elsevier.com/locate/chemphys

Calculation of ^{19}F NMR chemical shifts in uranium complexes using density functional theory and pseudopotentials

Michal Straka *,[1], Martin Kaupp *

Institut für Anorganische Chemie, Universität Würzburg, Am Hubland, D-97074 Würzburg, Germany

Received 31 March 2004; accepted 6 October 2004

Abstract

The ^{19}F NMR nuclear shieldings of fluoride ligands in uranium complexes UF_nCl_{6-n} ($n = 1$–6) have been studied quantum chemically, using different exchange-correlation functionals and a relativistic small-core pseudopotential on uranium. In contrast to a recent study [G. Schreckenbach, S.W. Wolff, T. Ziegler, J. Phys. Chem. A 104 (2000) 8244] we find that pseudopotential methods are well suited for calculations of ligand chemical shifts in actinide compounds, provided that a sufficiently small core-size definition is used. With modern relativistic small-core pseudopotentials and gradient-corrected density functionals we obtain results of the same accuracy as were found with all-electron density functional ZORA or Pauli calculations. The unusually large dependence of the shifts on the exchange-correlation functional is discussed in the context of the description of σ- and π-bonding, and also with respect to the accuracy of the optimized structures.

1. Introduction

Calculations of properties for heavy-element compounds require the inclusion of relativistic effects. This holds particularly for magnetic resonance parameters like NMR chemical shifts [1–3], which sample regions close to the nuclei in question. While four-component all-electron Dirac–Fock calculations of NMR chemical shifts have been carried out [4], the four-component methods are still restricted to uncorrelated methods and to very small molecules. Two-component or scalar relativistic all-electron methods have also been employed, based initially on the quasi-relativistic Pauli method (with frozen-core approximation [5]), more recently on the zeroth-order regular approximation (ZORA) [6], and also at the Douglas–Kroll–Hess (DKH) level [7]. ZORA and DKH methods appear currently as the methods of choice for the calculation of magnetic resonance parameters of the heavy nuclei themselves. Furthermore, we have shown about a decade ago [8], that replacement of the core electrons of a heavy atom by a relativistic pseudopotential (effective-core potential, ECP) allows the accurate and efficient inclusion of scalar relativistic effects into calculations of chemical shifts of neighboring, lighter nuclei. Spin–orbit (SO) effects may also be treated within this framework by using SO ECPs [9]. The accuracy of the ECP/SO-ECP approach was demonstrated in particular for ligand NMR chemical shifts in 5d transition metal complexes [8–10].

Recently, Schreckenbach et al. extended the theoretical calculation of NMR chemical shifts to the area of actinide systems [11,12]. They used all-electron ZORA and Pauli approaches for both ligand and metal shieldings, and they also tested ECP methods for ^{19}F shifts in UF_nCl_{6-n} ($n = 1$–6) complexes. They concluded that "the ECP approach is beyond its limits" for chemical shift calculations in actinide systems [11]. However, the uranium pseudopotential used in [11] was a large-core type ECP. The use of large-core ECPs has been found

* Corresponding authors.
E-mail addresses: straka@mail.uni-wuerzburg.de (M. Straka), kaupp@mail.uni-wuerzburg.de (M. Kaupp).
[1] Present address: Department of Chemistry, P.O. Box 55 (A.I. Virtasen aukio 1), University of Helsinki, FIN-00014, Helsinki, Finland.

0301-0104/$ - see front matter © 2004 Elsevier B.V. All rights reserved.
doi:10.1016/j.chemphys.2004.10.041

unreliable already for less sensitive properties, such as molecular structures, energetics, or vibrational spectra (see, e.g. [13,14]). This is particularly serious in the case of actinides, like uranium [15], which utilize 5f, 6d, and 7s orbitals in bonding, and which possess polarizable 6p semicore orbitals [16,17]. It appears thus doubtful whether it is appropriate to use large-core pseudopotentials in calculations of a sensitive property like nuclear shielding.

In this study, we show that an accurate relativistic small-core uranium pseudopotential provides results of the same quality as all-electron ZORA or Pauli methods for ^{19}F shieldings in UF_nCl_{6-n} ($n = 1$–6) complexes. Pseudopotentials do thus not appear to be a limiting factor for the accuracy of calculations of ligand chemical shifts in actinide complexes. This has allowed us to examine in more detail the performance of different density functionals, basis sets, and input structures in calculating ^{19}F nuclear shieldings in uranium complexes. We further discuss the influence of spin–orbit effects, solvation, and temperature on the shieldings.

2. Computational details

All calculations were done with the Gaussian 98 code [18]. We used scf = tight (energy and density matrix convergence 10^{-8}) and grid = ultrafine (75 radial shells and 302 angular points per shell; about 7000 points per atom) options to avoid numerical inaccuracies. Throughout this study we used the nine exchange-correlation functionals BP86, B3P86, BHP86, BLYP, B3LYP, BHLYP, BPW91, B3PW91, BHPW91. These are combinations of Becke88 (B) [19], Becke-3 (B3) [20] and Becke-half-and-half (BH) [21] exchange functionals including 0%, ca. 20%, and 50% Hartree–Fock (HF) exchange, respectively. These were combined with three correlation functionals, those of Perdew (P86) [22], Lee–Yang–Parr (LYP) [23], and Perdew–Wang (PW91) [24]. The ECPs and valence basis sets compared for uranium, as well as different all-electron basis sets used for F and Cl, are listed in Table 1. In addition to the Stuttgart-type relativistic small-core ECPs (RSC ECP) [25], we also used in some comparative shielding calculations the Los-Alamos type large-core ECPs (RLC ECP) [26] employed previously by Schreckenbach et al. [11].

2.1. Structures

It appears that the performance of different density functionals for structure optimization of actinide complexes has only been evaluated partially [15,27]. We therefore optimized the structures of UF_6 and UCl_6 with all nine functionals, using the RSC ECP on uranium. To further study basis set effects on structure, we re-optimized UF_6 for selected functionals with two additional g functions in the uranium basis set and with the aug-cc-PVTZ [28] basis set on F. The aug-cc-PVTZ basis set is close to the basis set limit for the DFT calculations. The structures of $UF_nCl_{(6-n)}$ ($n = 1$–6) series for shielding calculations were optimized at B3LYP, B3P86, and BHLYP levels using the default RSC valence basis set on uranium and TZVP [29] basis sets on F and Cl (see Table 1 for details).

2.2. Shieldings

The basis-set and ECP dependence of ^{19}F shieldings was studied for UF_6 at its experimental U–F distance (199.6 pm) [30]. For more details see Tables 5 and 1. The RSC ECP and RSC-spdf+2g valence basis set on uranium and IGLO-III basis set [31] on F and Cl, (cf. Table 1), were chosen for further shielding calculations. Gauge-including atomic orbitals (GIAO) [32] were used to deal with the gauge origin problem of the magnetic vector potential.

2.3. Reference shieldings

The conventional reference compound used experimentally for ^{19}F chemical shifts is bulk $CFCl_3$. The experimental ^{19}F absolute shielding in $CFCl_3$ has been given as 188.7 ppm [33]. Computed ^{19}F shieldings in the gas-phase $CFCl_3$ molecule with IGLO-III basis set (at B3LYP/TZVP optimized structure) are listed in Table 2. The results depend strongly on the amount of HF exchange in the functional and less on the correlation functional. The calculated ^{19}F shieldings range from ca. 125 ppm for the generalized gradient-corrected (GGA) Becke (B) functional, via ca. 155 ppm for the hybrid B3 functional (ca. 20% HF exchange) to ca. 185 ppm for the hybrid BH exchange functional (50% HF exchange). The Hartree–Fock value provides too large shielding, whereas the MP2 value is close to experiment. Probably this extreme method dependence of the shielding in this seemingly simple molecule is related to non-dynamical correlation effects arising from the small size and high electron density of the fluorine atom. Basis set effects on fluorine shielding in $CFCl_3$ were found to be less dramatic (cf. Table S1 in Supporting Information). To avoid possible inaccuracies due to the computation of reference shieldings, we decided to compare absolute fluorine shieldings. Experimental chemical shifts were thus converted to absolute shieldings using the experimental absolute shielding of $CFCl_3$ [33]. This removes any possible dependence of the reference value on computational level. The chemical shifts in ref. [11] were obtained with the help of computed $CFCl_3$ shieldings. We converted these data back to the original absolute shieldings for consistent comparison.

Solvation effects were studied at the continuum solvent level, using the conductor-like polarizable contin-

Table 1
Pseudopotentials (ECPs) and basis sets used in this study

Element	ECP	Basis set	Quality	Comments	References
U	RLC(14-VE)	RLC	6s5p2d4f	Uncontracted	[26]
	RLC(14-VE)	RLC+spdf+2g	7s6p3d5f2g	Uncontracted; diffuse spdf functions[a] and 2g functions[b] added	[26]
	RSC(32-VE)	RSC	12s11p10d8f/8s7p6d4f	Default basis set	[25]
	RSC(32-VE)	RSC-uncont.	12s11p10d8f	Uncontracted	[25]
	RSC(32-VE)	RSC+2g	12s11p10d8f2g/8s7p6d4f2g	g Functions[b] added	[25]
	RSC(32-VE)	RSC+spdf+2g	13s12p11d9f2g/9s8p7d5f2g	Diffuse spdf functions[a] and g functions[b] added	[25]
	RSC(32-VE)	RSC-spdf+2g	11s10p9d7f2g/7s6p5d3f2g	Most diffuse spdf set removed and g functions[b] added	[25]
F		TZVP	11s6p1d/5s3p1d		[29]
		aug-cc-PVTZ	11s6p3d2f/5s4p3d2f		[28]
		IGLO-II	9s5p1d/5s4p1d		[31]
		IGLO-III	11s7p2d/7s6p2d		[31]
		IGLO-III+f	11s7p2d1f/7s6p2d1f	$\alpha_F = 1.85$	[31]
		6-311+G(2df)	12s6p2d1f/5s4p2d1f		[11]
		Partridge-III	18s13p4d/18s13p4d	$\alpha_D = 4.3, 1.3, 0.4, 0.12$	[37]
		Partridge-III+f	18s13p4d1f/18s13p4d1f	$\alpha_F = 1.85$	[37]
Cl		TZVP	14s10p1d/5s4p1d		[29]
		IGLO-III	12s8p3d/8s7p3d		[31]

[a] Diffuse spdf-exponents were obtained by dividing the most diffuse exponents in the original basis set by a factor of 3.
[b] $\alpha_G = 1.18, 0.42$.

Table 2
Computed ^{19}F nuclear shieldings for $CFCl_3$[a]

Method	σ (ppm)
BP86	123.2
BLYP	123.8
BPW91	124.8
B3P86	151.6
B3LYP	150.8
B3PW91	151.9
BHP86	184.6
BHLYP	184.5
BHPW91	186.4
HF	230.0
MP2	193.7

[a] At B3LYP/TZVP optimized structure, using IGLO-III basis set. Experimental value 188.7 ppm [33].

uum model (CPCM) [34] as implemented in Gaussian 98. We optimized the structures at the B3LYP/RSC-TZVP level in CCl_4 solvent ($\varepsilon = 2.228$) and then calculated the shieldings using the same solvent.

Natural bond orbital and population analyses [35] employed the built-in NBO-3.1 subroutines of the Gaussian 98 program.

3. Results and discussion

3.1. Molecular structures

3.1.1. Performance of different functionals for UF_6 and UCl_6

Experimentally, the molecular structure of the molecules studied here is known only for UF_6. We therefore have to rely on computed structures in our shielding calculations. In view of the unusually large dependence of computed shieldings on U–X bond lengths (see below), this is a potential error source in the shielding calculations. Previous computational studies of structures and vibrational spectra of actinide systems appear to have favored B3-type hybrid functionals over GGA functionals [27]. BH-type hybrid functionals do not seem to have been employed before. U–X bond lengths optimized for UF_6 and UCl_6 with different functionals (at the RSC ECP level) are listed in Table 3. We observe non-negligible, systematic differences between the functionals. The more HF exchange in the functional, the shorter is the U–X bond. The P86 and PW91 correlation functionals lead to similar bond lengths while LYP gives slightly longer bonds. Extension of the uranium valence basis set by two g-functions shortens the bond by about 0.6–0.7 pm. Use of the very large aug-cc-PVTZ basis set on fluorine changes the bond lengths only by about 0.1 pm. The TZVP fluorine basis set seems thus to be well suited for structure optimization. Overall, it appears that the B3-type hybrid functionals provide results in reasonable agreement with experiment for UF_6, whereas BH-type hybrid functionals give shorter and gradient-corrected functionals give longer bonds.

3.1.2. The $UF_nCl_{(6-n)}$ ($n = 1$–6) series

The molecular structures of the $UF_nCl_{(6-n)}$ ($n = 1$–6) series were optimized with the RSC ECP and RSC basis set on U and the TZVP basis set on F and Cl using (a) The B3LYP functional to be able to compare with previous work, (b) the B3P86 functional, as the B3P86/RSC-TZVP level provided particularly good

Table 3
Optimized U–F(Cl) bond lengths (in pm) for UF_6 and UCl_6 using various basis sets and functionals[a]

Method	UF_6			UCl_6
	RSC,TZVP	RSC+2g,TZVP	RSC+2g,aug-cc-PVTZ	RSC,TZVP
BP86	202.5			248.1
BLYP	204.1	203.4	203.5	251.0
BPW91	202.5			247.9
B3P86	199.8	199.1		244.9
B3LYP	201.2	200.5	200.6	247.5
B3PW91	200.0	199.4		245.3
BHP86	197.4			242.4
BHLYP	198.7	198.1	198.2	244.7
BHPW91	197.4			242.2
Experimental	199.6[b], 199.8[c]			

[a] Cf. Table 1 and computational details for descriptions of basis sets and ECPs.
[b] Ref. [30].
[c] See H.M. Seip, Acta Chem. Scand. 20 (1965) 2698.

agreement with experiment for UF_6 (see above), and (c) the BHLYP functional for further comparisons. The optimized U–F(Cl) bond lengths are listed in Table 4. All homoleptic complexes were found to be octahedral, and the heteroleptic complexes exhibit angles close to those for the octahedral systems (cf. Cartesian coordinates provided in Tables S2 and S3 in Supporting Information). All systems were found to be minima on the potential energy surface at all computational levels evaluated. While we reproduce largely the trends in bond lengths observed by Schreckenbach [36], our distances are somewhat shorter. This is most likely due to the more accurate RSC ECPs and basis sets used here, compared to the RLC ECP calculations in [36]. Fluorine atoms *trans* to another fluorine atom exhibit shorter U–F distances than those *trans* to a chlorine atom (the differences are small but systematic). Similarly, the U–Cl distances *trans* to Cl are longer than *trans* to F. Again (cf. above for UF_6), the LYP correlation functional gives longer distances than P86, and the BH exchange functional gives shorter distances than B3.

Table 4
Optimized bond lengths (pm) in UF_nCl_{6-n} ($n = 1$–6)[a,b] at different DFT levels

	Symmetry	Parameter[c]	B3P86	B3LYP	BHLYP
UF_6	O_h	U–F	199.8	201.2	198.7
UF_5Cl	C_{4v}	U–F_{tF}	199.4	200.9	198.3
		U–F_{tCl}	199.7	201.2	198.6
		U–Cl	246.6	248.9	246.4
trans-UF_4Cl_2	D_{4h}	U–F	199.0	200.5	197.9
		U–Cl	246.6	248.9	246.4
cis-UF_4Cl_2	C_{2v}	U–F_{tF}	199.0	200.6	198.0
		U–F_{tCl}	199.4	200.8	198.3
		U–Cl	246.2	248.7	246.0
mer-UF_3Cl_3	C_{2v}	U–F_{tF}	198.6	200.2	197.5
		U–F_{tCl}	198.9	200.4	197.7
		U–Cl_{tCl}	246.2	248.6	246.0
		U–Cl_{tF}	245.7	248.2	245.5
fac-UF_3Cl_3	C_{3v}	U–F	199.0	200.5	197.9
		U–Cl	245.8	248.3	245.6
trans-UF_2Cl_4	D_{4h}	U–F	198.1	199.8	197.0
		U–Cl	245.7	248.2	245.5
cis-UF_2Cl_4	C_{2v}	U–F	198.5	200.0	197.4
		U–Cl_{tCl}	245.8	248.3	245.6
		U–Cl_{tF}	245.2	247.9	245.1
$UFCl_5$	C_{4v}	U–F	198.1	199.6	196.8
		U–Cl_{tCl}	245.4	247.9	245.1
		U–Cl_{tF}	244.9	247.5	244.7
UCl_6	O_h	U–Cl	244.9	247.5	244.7

[a] RSC-ECP-TZVP basis sets.
[b] Cartesian coordinates given in Supporting Information.
[c] Subscript tF = *trans* to fluorine. Subscript tCl = *trans* to chlorine.

Table 5
Basis set effects on ^{19}F shielding (ppm) in UF_6[a]

Metal	Ligand					
	6-311+G(2df)	IGLO-II	IGLO-III	IGLO-III+f	Partridge-III	Partridge-III+f
RLC	−789.9	−812.2	−812.8	−807.4	−827.1	−813.0
RLC+spdf+2g	−775.4	−789.3	−805.0	−800.3	−819.5	−819.8
RSC	−658.2	−675.5	−673.9	−671.6	−677.3	−675.1
RSC-uncontracted	−656.2	−673.0	−671.9	−669.8	−675.5	−673.4
RSC+2g	−647.6	−661.1	−667.2	−665.3	−670.6	−669.0
RSC+spdf+2g	−647.6	−661.2	−667.2	−665.4	−670.6	−670.6
RSC-spdf+2g	−647.7	−660.9	−667.2	−665.4	−670.6	−669.0

[a] B3LYP results for experimental structure. Cf. Table 1 and computational details for descriptions of basis sets and ECPs.

3.2. Basis set effects on shielding

Initial studies of basis set effects on calculated shieldings used the B3LYP functional on UF_6 at its experimental structure. Due to potential error sources from structure, ro-vibrational or environmental effects, we prefer to compare at this point not to experiment but theory against theory, with the very large Partridge-III+f basis set for fluorine [37] (cf. Table 1) as a reference case. The shieldings calculated with the large-core ECP on uranium are systematically about 150 ppm lower than the small-core ECP results (Table 5). Improving the basis set for the RLC ECP by diffuse (1s, 1p, 1d, 1f) and polarization (2g) functions does not change this trend dramatically. Such large differences reflect clearly significant deficiencies of the RLC ECP (as shown below, the RSC ECP result compare favorably with all-electron data).

Contraction errors of the default uranium RSC basis set are small: complete uncontraction increases shieldings by only 2–3 ppm. Addition of two g-functions on uranium increases the shielding by about 5–10 ppm. Augmentation by an additional diffuse spdf set (RSC+spdf+2g basis set in Tables 1 and 5) changes the results by less than 1 ppm, suggesting that the default valence basis set is essentially saturated in the spdf space. Indeed, removal of the most diffuse spdf set from the default basis (RSC-spdf+2g) also has an influence of less than 1 ppm. As has been found earlier, the IGLO-III basis on fluorine is already close to the extended Partridge reference value, whereas IGLO-II exhibits slightly larger deviations of a few ppm. Addition of f-functions on fluorine increases the shielding by about 2 ppm. The 6-311+G(2df) basis set employed by Schreckenbach et al. [11] performs already appreciably worse, giving ca. 20 ppm too high shielding. In the remainder of this work we will concentrate on the small-core ECP with contracted RSC-spdf+2g valence basis set for uranium, with the IGLO-III basis on F and Cl. This level is expected to provide good accuracy at reasonable computational effort, with estimated basis-set errors in calculated shieldings of less than 10 ppm.

3.3. Comparison of ECP and all-electron results for ^{19}F shieldings

Proceeding to the $UF_nCl_{(6-n)}$ ($n = 1$–6) series, Table 6 compares all-electron and large-core ECP results from

Table 6
Experimental and calculated ^{19}F shieldings for the UF_nCl_{6-n} ($n = 1$–6) series

System	Position[a]	Experimental[b]	ZORA (scalar)/PW91[c]	ZORA/PW91[c]	Pauli (scalar)/PW91[c]	Pauli/PW91[c]	RSC/BPW91[d]	RSC/B3LYP[d]	RLC/B3LYP[c]
UF_6	F_{tF}	−575.3	−726.0	−700.3	−681.8	−715.9	−730.8	−706.2	−875.3
UF_5Cl	F_{tF}	−573.3	−706.4	−682.6	−661.8	−694.3	−719.0	−692.6	−831.5
	F_{tCl}	−592.8	−671.8	−649.5	−627.1	−667.2	−686.3	−689.0	−845.3
trans-UF_4Cl_2	F_{tF}	−566.8	−697.2	−674.3	−651.7	−682.4	−710.9	−684.2	−795.4
cis-UF_4Cl_2	F_{tF}	−571.3	−694.1	−672.6	−648.4	−680.3	−710.0	−682.7	−800.7
	F_{tCl}	−597.1	−656.8	−636.6	−611.0	−649.0	−672.4	−672.9	−812.6
mer-UF_3Cl_3	F_{tF}	−564.3	−687.7	−667.3	−642.6	−673.3	−704.9	−678.0	−763.9
	F_{tCl}	−593.9	−646.3	−628.3	−600.3	−636.6	−664.4	−664.7	−770.6
fac-UF_3Cl_3	F_{tCl}	−597.7	−644.0	−627.3	−597.1	−632.6	−662.8	−662.6	−771.7
trans-UF_2Cl_4	F_{tF}	−557.4	−682.9	−664.3	−639.0	−668.7	−701.4	−675.6	−733.9
cis-UF_2Cl_4	F_{tCl}	−592.3	−639.7	−624.6	−593.3	−627.0	−657.4	−657.8	−741.6
$UFCl_5$	F_{tCl}	−585.6	−632.2	−620.1	−587.4	−620.3	−653.6	−655.5	−703.1

[a] F_{tF} = fluorine *trans* to another fluorine. F_{tCl} = fluorine *trans* to chlorine.
[b] Experimental results from A.J. Downs, C.J. Gardner, J. Chem. Soc., Dalton Trans. (1984) 2127.
[c] ZORA, Pauli and RLC-ECP results from [11].
[d] This work: RSC-ECP results with IGLO-III basis on ligands, using B3LYP/RSC-TZVP optimized structures.

Table 7
Dependence of ^{19}F shieldings in the UF_nCl_{6-n} ($n = 1$–6) series on exchange-correlation potential[a]

System	Position[b]	BP86	BLYP	BPW91	B3P86	B3LYP	B3PW91	BHP86	BHLYP	BHPW91	Experimental
UF_6	F_{tF}	−727.0	−726.7	−730.8	−710.3	−706.2	−709.8	−611.2	−606.7	−612.6	−575.3
UF_5Cl	F_{tF}	−714.6	−707.2	−719.0	−702.0	−692.6	−703.0	−618.3	−606.2	−620.3	−573.3
	F_{tCl}	−682.0	−674.3	−686.3	−696.4	−689.0	−696.6	−633.7	−629.0	−635.0	−592.8
trans-UF_4Cl_2	F_{tF}	−705.9	−693.1	−710.9	−697.8	−684.2	−700.0	−629.7	−611.1	−632.1	−566.8
cis-UF_4Cl_2	F_{tF}	−705.1	−692.6	−710.0	−695.8	−682.7	−697.9	−624.4	−606.7	−626.7	−571.3
	F_{tCl}	−667.6	−654.5	−672.4	−684.8	−672.9	−686.3	−639.6	−627.5	−641.3	−597.1
mer-UF_3Cl_3	F_{tF}	−699.7	−683.2	−704.9	−694.1	−678.0	−697.2	−635.4	−613.0	−638.2	−564.3
	F_{tCl}	−659.1	−642.0	−664.4	−680.2	−664.7	−682.9	−654.2	−635.8	−656.5	−593.9
fac-UF_3Cl_3	F_{tCl}	−657.6	−640.7	−662.8	−677.7	−662.6	−680.3	−645.7	−628.2	−647.9	−597.7
trans-UF_2Cl_4	F_{tF}	−695.9	−676.5	−701.4	−693.9	−675.6	−697.7	−645.9	−620.0	−649.1	−557.4
cis-UF_2Cl_4	F_{tCl}	−651.8	−631.8	−657.4	−675.6	−657.8	−679.1	−659.3	−636.7	−662.0	−592.3
UF_5Cl	F_{tCl}	−647.8	−625.4	−653.6	−675.3	−655.5	−679.6	−671.5	−645.2	−674.6	−585.6

[a] RSC ECP results with IGLO-III basis on ligands, at B3LYP/RSC-TZVP optimized structures.
[b] F_{tF} = fluorine *trans* to another fluorine. F_{tCl} = fluorine *trans* to chlorine.

[11] and some of our present small-core ECP results to experiment (small-core ECP results with other functionals are given in Table 7). We will concentrate initially on the scalar relativistic results. As the all-electron results of [11] were restricted to GGA functionals, it is appropriate to compare to our GGA results. Fig. 1 shows that the small-core ECP calculations, unlike the large-core ECP data, provide results close to the scalar relativistic all-electron ZORA and Pauli calculations (our ECP data in Table 6 used the B88 functional rather than the PW91 functional for exchange, but that affects the results negligibly, as can be seen from Table S9 in Supporting Information). It is thus not the pseudopotential approximation in general but the choice of a large-core ECP in [11] that led to large errors in the shielding calculations. Indeed, at the RSC ECP level, not the ECP but other factors like the exchange-correlation potential or the input structure appear to limit the achievable accuracy (see below). The direct plot of computed against experimental data chosen for Fig. 1 shows also that even the hybrid B3LYP functional *does not* describe the experimental trends correctly as previously concluded in [11]. In general, all conclusions drawn from the RLC ECP results have to be considered doubtful.

SO contributions to the ^{19}F shieldings are relatively small [11,12]. This is understandable due to the relatively small fluorine s-character in the U–F bond [1,38], as discussed before [11,12]. While the SO effects were of opposite sign at ZORA and Pauli levels [11] as seen from Table 6 (cf. Figure S1 in Supporting Information), they are apparently relatively constant for all species and thus are expected to affect the shielding trends only little (as a small caveat, we cannot rule out completely that at other computational levels SO effects may make non-negligible contributions to the deviations from experiment). Our preliminary results [39], using the SO-ECP approach of [9], are similar to the Pauli data, that is deshielding by ca. 25–35 ppm. It is not straightforward

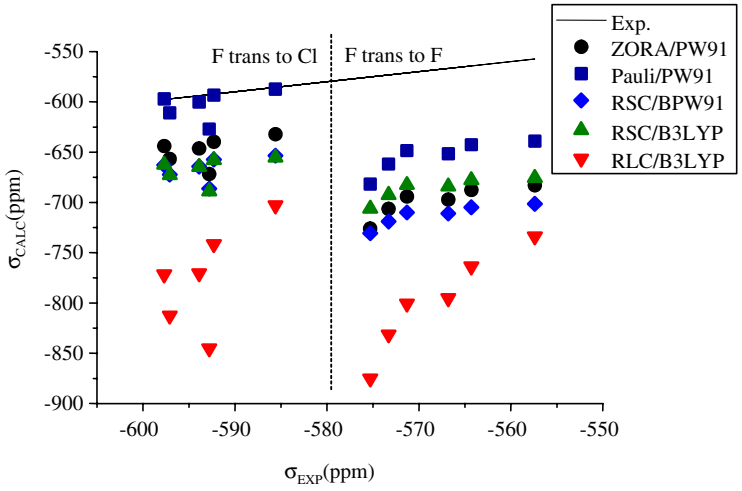

Fig. 1. Comparison of the present small-core ECP results on ^{19}F shieldings with large-core ECP and all-electron ZORA and Pauli results from [11] (cf. Table 6). Only scalar relativistic results are shown.

in the present case to predict from general arguments what the correct sign of the SO shifts should be: In related octahedral transition metal complexes, the predominant SO contributions arise from occupied t_{2g}-type MOs [9]. These are π-antibonding relative to the metal-ligand bond and make thus shielding SO contributions [1,9]. In contrast, contributions from orbitals with σ-character relative to the M–L bond are known to provide deshielding SO effects [1,9]. As our analyses in the present case show that MOs with both σ- and π-character contribute to the SO shifts (see also below), partly compensating contributions of opposite sign are expected. This may explain the sensitivity to the relativistic method employed.

3.4. Comparison of different exchange-correlation potentials

Assuming thus that the neglected SO effects do not explain the main deviations from experiment, we have to worry about the exchange-correlation potentials employed. One of the most striking observations in the comparison with experiment (Fig. 1) is the existence of two distinct groups of fluorine atoms: results for fluorine nuclei *trans* to another fluorine (F_{tF}) follow the experimental trends more or less but underestimate experimental shieldings significantly. Fluorine nuclei *trans* to chlorine (F_{tCl}) are overall closer to ideal agreement with experiment but exhibit larger scatter. Most notably, the fact that the F_{tCl} shieldings are experimentally lower than the F_{tF} shieldings is not reproduced at the GGA level, neither in all-electron nor in ECP calculations (cf. Fig. 1). While this "step" in the plots is somewhat reduced at the B3LYP level, the correct order is not restored.

The full set of ^{19}F shieldings obtained at RSC ECP level with nine different density functionals is summarized in Table 7. An appreciable dependence on the functional is seen. As for structures and shieldings of UF_6 (see above), results with the LYP correlation functional deviate somewhat from the PW91 and P86 data (shieldings are somewhat larger). The largest dependence exists, however, on the amount of HF exchange. This is shown clearly in Fig. 2, where BPW91, B3PW91, and BHPW91 results are compared (plots with the P86 correlation functional are almost identical, those with the LYP functional are shifted to somewhat larger shieldings). In all cases, the two distinct groups F_{tCl} and F_{tF} are notable. The step between these two groups, and thus the erroneous inversion of the experimental difference between them, is reduced upon increasing the HF exchange contribution. Thus, with BH-type hybrid functionals the correct behavior is finally restored, that is the F_{tCl} shieldings tend to be lower than the F_{tF} shieldings (cf. Table 7, Fig. 2). However, the trends within the two groups are also affected by the amount of HF exchange. While the shieldings within the F_{tCl} group are scattered also with BH-type functionals, the F_{tF} shieldings exhibit now a decrease with increasing chlorine substitution, in disagreement with the experimental trend. The reasons for this admittedly relatively weak trend (the shieldings within the F_{tF} group cover only ca. 20 ppm) are not clear (see also below).

Further details that may be extracted from Table 7 are: (a) differences of LYP vs. P86 or PW91 results grow slightly with increasing chlorine substitution, and they are larger for the F_{tCl} group. The smallest dependence of the shieldings on the correlation functional is thus obtained for UF_6 and the largest for $UFCl_5$ (a graphical comparison of different correlation functionals is given in Figure S2 in Supporting Information).

Schreckenbach et al. noted that, while their isotropic shieldings at GGA levels were too deshielded relative to experiment, the shielding anisotropy for UF_6 of ca. 1215–1270 ppm (depending on the relativistic treatment)

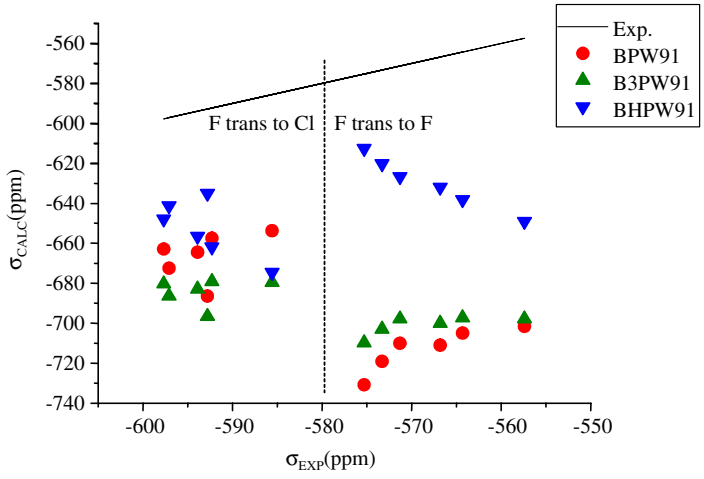

Fig. 2. Dependence of ^{19}F shieldings on HF exchange admixture (RSC ECP results, cf. Table 7).

coincided well [11] with the experimental value of 1210 ± 30 ppm [40]. We find anisotropies of ca. 1250–1270 ppm for GGA functionals, of ca. 1320–1350 ppm with B3-type and BH-type hybrid functionals (depending on correlation functional and basis set). Thus, the agreement with experiment for the shielding anisotropy actually deteriorates somewhat upon HF-exchange admixture.

3.5. Structural dependence of shieldings

In view of the large paramagnetic contributions to the ^{19}F shieldings in the uranium complexes studied, we may expect a relatively large dependence of the shieldings on the U–X bond lengths. While the results in Table 7 have been obtained for the B3LYP(RSC,TZVP) structures, we have also studied other levels for optimization of input structures. Recall, that increasing HF exchange shortens the U–X bond lengths, and the LYP correlation functional provides slightly longer bonds than the PW91 or P86 functionals (cf. Section 3.1, Table 3).

As a first test, we compared the shieldings for UF_6 at the 201.2 pm U–F bond length obtained at our standard B3LYP/RSC-TZVP level employed and those computed at the experimental distance of 199.6 pm. Shortening of the U–F distance by only these 1.6 pm decreases the shielding by about 35–40 ppm for all nine functionals (cf. Table S4 in Supporting Information). This corresponds to a shielding gradient of about -20 to -30 ppm/pm (Schreckenbach found a gradient of ca. -18 ppm/pm [11]). Notably, the results for the experimental structure are closer to the experimental UF_6 shielding of -575.3 ppm. A large dependence of calculated shieldings on bond length was already noted by Schreckenbach et al. [11].

We also used B3P86/RSC-TZVP and BHLYP/RSC-TZVP optimized structures for the entire $UF_nCl_{(6-n)}$ series in comparison with the results of Table 7. The shortening of the U–X bond lengths at these levels by 1.4–1.7 and 2.5–2.8 pm (cf. Table 4) increases the shieldings by ca. 30–35 and 40–60 ppm, respectively (see Tables S5, S6 and Figure S3 in Supporting Information). However, at a given level of shielding calculation, the trends for different compounds are not changed notably. Errors in the optimized structures may thus affect the shifts systematically and significantly but can probably not explain the remaining discrepancies of the shielding trends relative to experiment (unless *all* of the functionals misrepresent the relative magnitude of the U–F_{tF} vs. U–F_{tCl} bond lengths, which we consider unlikely).

3.6. Solvation and temperature effects

As the experimental data were obtained near -60 °C in $CFCl_3$, we also have to consider solvation and temperature effects on the shieldings. Given the large dependence of the shieldings on U–X bond lengths (see above), rovibrational effects are expected to be non-negligible but probably will not notably affect the computed trends. Experimentally, the temperature effects on shielding for UF_6 were found to be very small, ca. 0.05 ppm/degree [41]. We expect that the temperature will not affect the trends dramatically for the series of complexes studied. The temperature dependence was found to be relatively large for methoxy-substituted uranium fluorides [41], but this has been attributed to the formation of charge-transfer complexes with the solvent.

As a rough estimate of solvation effects, we carried out structure optimizations and subsequent shielding calculations in a continuum solvent model (CPCM level, see Computational Details). We observed almost no influence on structures (changes within 0.1 ppm) and very little influence on the shieldings. That is, the overall effect is less than 1 ppm and less than 6 ppm for UF_6 and UF_2Cl_4, respectively (cf. Tables S7 and S8 in Supporting Information).

3.7. Interpretation of the dependence of shieldings on exchange-correlation functional, bonding analysis

The results in Section 3.4 revealed a rather large dependence of the computed shieldings on the exchange-correlation potential, in particular on the admixture of HF exchange. Moreover, the overall agreement with experiment for any of the potentials used is far from the accuracy we find, e.g., for ligand chemical shifts in transition metal complexes. For example, calculations at similar computational levels as used here for the ^{19}F shieldings in the $WF_nCl_{(6-n)}$ ($n = 1$–6) series [39] exhibit much smaller dependencies on the functional and reproduce well the experimentally observed trends. Notably, in 4d or 5d transition metal $MF_nCl_{(6-n)}$ complexes, the overall trends differ also experimentally from those found for the analogous uranium systems, e.g., the shielding is larger for fluorines *trans* to chlorine than for those *trans* to fluorine [42]. The opposite behavior of the uranium complexes, which obviously is so hard to reproduce theoretically, is most likely related to the strong involvement of f-orbitals in bonding.

As has been discussed previously, one consequence of the 5f-orbital involvement in bonding to actinides is a strengthening and shortening of bonds to ligands like fluoro, chloro or oxo groups, due to strong π(f-p) bonding [17]. It appears (see below) that the character of this π-donation from ligand lone-pair orbitals into uranium 5f-orbitals depends strongly on the theoretical description, in particular on the exchange-correlation functional. This sensitivity explains probably the appreciable dependence of the bond lengths on HF-exchange admixture (see Section 3.1), and it may contribute also to the sensitivity of the computed shieldings on

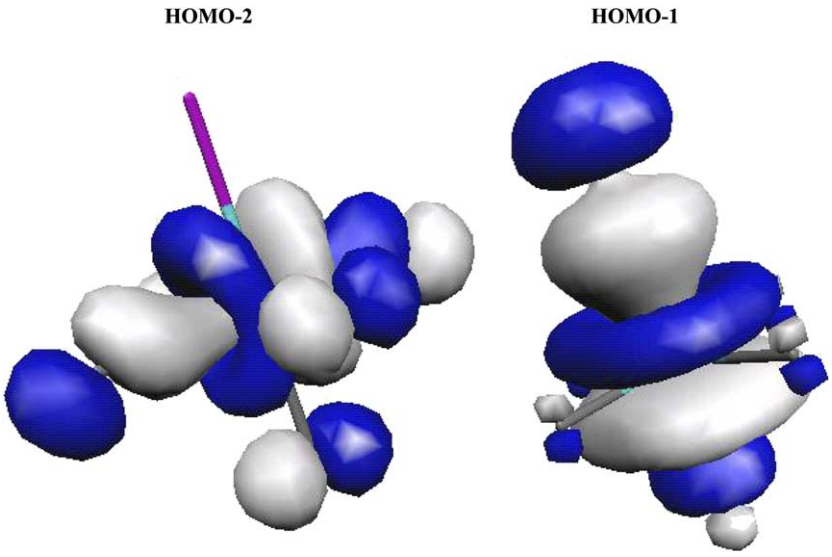

Fig. 3. Isosurface plot (±0.05 a.u. level) of frontier molecular orbitals of UF_5Cl. Only one component of the twofold degenerate HOMO-2 is shown.

the exchange-correlation potential. In addition, Schreckenbach et al. [11] suggested differential changes in orbital energies upon HF exchange admixture to be responsible for the modification of the shielding trends in the $UF_nCl_{(6-n)}$ series. Due to the presence of coupling terms in the case of non-local hybrid potentials, these effects are difficult to unravel. We have recently suggested that use of "localized hybrid potentials" within an optimized effective potential framework will not only improve the general numerical performance in shielding calculations but also simplify the relation to the one-electron orbitals [43] (see also [44]). Use of these potentials for the present uranium complexes is outside the scope of the present study and will be pursued elsewhere.

Closer analysis of the shieldings (data not shown; the analyses employed our in-house property package MAG-ReSpect [45]) shows that the largest contributions to the paramagnetic part of the ^{19}F shieldings arise from couplings between the frontier orbitals (which exhibit small energy denominators in the second-order perturbation expression for paramagnetic shielding). These have all appreciable 5f-character on uranium [36]. While the occupied orbitals are either U–F σ- or π-bonding, the lowest unoccupied MOs may be either metal centered and nonbonding (these will contribute less to the ^{19}F shieldings) or U–F antibonding. It is thus clear, that the shieldings will strongly depend on the description of U–F(Cl) bonding, which is complicated by the simultaneous involvement of 5f, 6d, and 7s orbitals in bonding.

Schreckenbach et al. suggested that the energies of the occupied MOs (less so the virtual ones) will be affected by HF exchange admixture. Moreover, coupling terms will come into play [11]. A closer analysis of the canonical MO contributions for UF_5Cl from our RSC ECP calculations provides more insight. While a full MO analysis is rendered exceedingly complicated by the presence of many large contributions with opposite sign, we have been able to single out two sets of occupied MOs that may explain the change of the relative F_{tF} vs. F_{tCl} shifts. Fig. 3 shows isosurface plots for HOMO-1 and HOMO-2. HOMO-1 has a_1 symmetry and exhibits U–Cl and U–F_{tCl} bonding character. It provides a very large deshielding contribution of −267 ppm to σ(F_{tCl}) but negligible contributions to σ(F_{tF}) (BP86 result with common gauge on uranium). The degenerate HOMO-2 (e-symmetry; only one component is shown) exhibits σ(U–F_{tF}) bonding character. The

Table 8
Dependence of NPA charges and NAO populations in UF_5Cl on functional[a]

Functional	U[b]	F_{tF}[c]	F_{tCl}[c]	Cl[c]	F_{tF}/F_{tCl}[d]	F_{tCl}/Cl[d]
BLYP	2.63(0.15s+0.45d+2.78f)	−0.47	−0.49	−0.26	1.04	1.89
B3LYP	2.85(0.15s+0.46d+2.54f)	−0.50	−0.52	−0.30	1.04	1.73
BHLYP	3.17(0.15s+0.46d+2.20f)	−0.56	−0.58	−0.36	1.04	1.61

[a] RSC-ECP(TZVP) results.
[b] NPA charge with populations in parentheses.
[c] NPA charge.
[d] NPA charge ratio.

Table 9
Analysis of NAO composition of selected NLMOs in UF_5Cl; dependence on functional[a]

NLMO	Functional	Uranium NAO contribution (%)	U NAO composition (%)			
			s	p	d	f
$U–F_F$	BLYP	12.5	4.8	0.3	10.8	84.1
	B3LYP	11.5	5.3	0.4	12.4	81.8
	BHLYP	10.6	6.0	0.3	14.2	79.7
$U–F_{tCl}$	BLYP	12.2	5.6	0.3	13.7	80.4
	B3LYP	11.7	6.0	0.3	14.9	78.8
	BHLYP	10.8	6.8	0.3	16.8	76.1
U–Cl	BLYP	19.2	12.0	0.2	10.1	77.6
	B3LYP	19.2	12.3	0.3	11.2	76.2
	BHLYP	18.8	13.0	0.5	13.1	73.6
$LP_\pi F_{tF}$	BLYP	5.8	0.0	0.4	17.7	81.9
	B3LYP	5.4	0.0	0.1	18.5	81.4
	BHLYP	4.9	0.0	0.2	19.5	80.4
$LP_\pi F_{tCl}$	BLYP	6.3	0.0	0.1	18.9	81.1
	B3LYP	5.7	0.0	0.6	20.0	79.4
	BHLYP	4.7	0.0	0.4	20.5	79.0
$LP_\pi Cl$	BLYP	9.6	0.0	0.1	10.5	89.4
	B3LYP	9.1	0.0	3.5	11.9	84.5
	BHLYP	6.7	0.0	1.5	12.6	79.9

[a] RSC-ECP(TZVP) results.

component displayed contributes −221 ppm to the shielding of two F_{tF} nuclei and −32 ppm to the shieldings of the other two F_{tF} nuclei (B86 results; the other component of the e-set contributes the same amount to the two remaining F_{tF} shieldings), but very little to $\sigma(F_{tCl})$. While coupling terms make the analysis more difficult for hybrid potentials, we may follow the change in MO energies of these two sets with HF exchange admixture: The HOMO-2 set is stabilized by ca. 0.16 a.u. from BLYP to BHLYP, similar to most of the other valence MOs. In contrast, the stabilization of the HOMO-1 is only 0.12 a.u. Thus, we expect that HF exchange admixture will reduce the deshielding less for the F_{tCl} position than for the F_{tF} position, as is observed. These findings provide support for the assumption that changes in the energies of the occupied MOs may be responsible for the dependence of the shielding trends on HF exchange admixture. The wrong trend within the F_{tF} group for BH-type functionals may suggest that the substitution pattern affects the stabilization of these types of σ-bonding MOs.

To see if the bond ionicity may affect the trends via the matrix elements of the perturbation expression for paramagnetic shielding (more precisely via the paramagnetic nuclear-spin–electron-orbit – PSO-matrix element [46]), we have furthermore performed NBO analyses for UF_5Cl. As shown clearly by the NPA populations and charges in Table 8, increasing HF exchange admixture makes the bonds more ionic, as is well known also for transition metal complexes [47]. Interestingly, this affects exclusively the uranium 5f contributions, while the 6d and 7s populations remain essentially constant. The significant change of computed shielding trends by HF exchange admixture (see Section 3.4) might suggest that this increased ionicity and the associated changes in orbital character and energies are not uniform for all bonds. This is confirmed by the NPA/NLMO analyses in Table 9: While all LMOs loose metal 5f contributions (and gain more relative 6d character) upon increasing HF exchange admixture, this is most pronounced for the π(U–Cl) bond (labelled as $LP_\pi(Cl)$). The competition of the π(U–Cl) bonds with the U–F σ- and π-bonds in *cis* and *trans* position should be affected differently by the lower covalency of the U–Cl π-bond upon HF exchange admixture. However, the changes seem to be too small to be notable in the results of Table 9. This suggests that the effects of changes in the orbital energies may be more important for the relative ordering of F_{tF} and F_{tCl} shieldings than the magnitude of the PSO matrix elements. We note in passing that our NPA/NLMO analyses indicate much higher f-character in the bonds than Schreckenbach's Mulliken analyses [36].

4. Conclusions

The results of the present study have shown clearly that an effective core potential on uranium provides comparable accuracy in calculations of ligand NMR chemical shifts in uranium complexes as computationally more demanding relativistic all-electron ZORA methods, provided that a sufficiently small core-size definition is used. The opposite conclusions drawn in [11] are due to the too large ECP core size used in that study. The availability of reliable ECP-based approaches demonstrated here opens the way to ligand chemical shift calculations on larger actinide complexes.

Small-core ECPs may furthermore be employed with quantum chemical programs that allow use of a larger variety of quantum chemical methods (different exchange-correlation functionals, Hartree–Fock or post-Hartree–Fock methods) for shielding calculations than the ADF code used by Schreckenbach et al. We have therefore been able to scrutinize the dependence of the ^{19}F shieldings in the $UF_nCl_{(6-n)}$ series on the exchange-correlation functional. We found a large effect of HF exchange admixture in hybrid functionals. While BH-type hybrid functionals recover the experimentally observed larger shieldings for the fluorine nuclei *trans* to another fluoride ligand compared to those *trans* to chlorine, the experimental shielding trends within the former group are actually reproduced less accurately at this level. Closer inspection of MO contributions suggests that it is mainly the relative stabilization of relevant U–F-bonding MOs by HF exchange admixture that is responsible for the large dependency of the computed trends on the exchange-correlation potential. Further analyses, in comparison with analogous transition metal complexes, are underway [39].

Acknowledgement

This project has been funded by Deutsche Forschungsgemeinschaft (project KA 1187/5-1). The graduate college "Modern Methods in Magnetic Resonance" at Stuttgart University is gratefully acknowledged for support of M.S.

Appendix A. Supplementary data

Nine tables and three figures with additional information on structures and shieldings are available. Supplementary data associated with this article can be found, in the online version, at doi:10.1016/j.chemphys.2004.10.041.

References

[1] M. Kaupp, Relativistic effects on NMR chemical shifts, in: P. Schwerdtfeger (Ed.), Relativistic Electronic Structure Theory II: Applications, Series Theoretical and Computational Chemistry, Elsevier, Amsterdam, 2004.

[2] M. Kaupp, O.L. Malkina, V.G. Malkin, NMR of transition metal compounds, in: P.v.R. Schleyer (Ed.), Encyclopedia of Computational Chemistry, Wiley Interscience, New York, 1998, p. 1857;
M. Bühl, M. Kaupp, V.G. Malkin, O.L. Malkina, J. Comput. Chem. 20 (1999) 91;
G. Schreckenbach, T. Ziegler, Theor. Chem. Acc. 99 (1998) 71;
J. Autschbach, T. Ziegler, Relativistic computation of NMR shieldings and spin–spin coupling constants, in: D.M. Grant, R.K. Harris (Eds.), Encyclopedia of Nuclear Magnetic Resonance, vol. 9, Wiley, Chichester, 2002;
J. Autschbach, T. Ziegler, Coord. Chem. Rev. 238/239 (2003) 83.

[3] See also various chapters in: M. Kaupp, M. Bühl, V.G. Malkin (Eds.), Calculation of NMR and EPR Parameters. Theory and Applications, Wiley-VCH, Weinheim, 2004.

[4] L. Visscher, T. Enevoldsen, T. Saue, H.J.A. Jensen, J. Oddershede, J. Comput. Chem. 20 (1999) 1262;
T. Enevoldsen, L. Visscher, T. Saue, H.J.A. Jensen, J. Oddershede, J. Chem. Phys. 112 (2000) 3493;
R. Fukuda, M. Hada, H. Nakatsuji, J. Chem. Phys. 118 (2003) 1015;
H.M. Quiney, H. Skaane, I.P. Grant, Chem. Phys. Lett. 290 (1998) 473;
S.S. Gómez, R.H. Romero, G.A. Aucar, J. Chem. Phys. 117 (2002) 7942.

[5] G. Schreckenbach, T. Ziegler, Int. J. Quantum Chem. 61 (1997) 899;
For a more complete implementation, see: R. Bouten, E.J. Baerends, E. van Lenthe, L. Visscher, G. Schreckenbach, T. Ziegler, J. Chem. Phys. 104 (2000) 5600.

[6] S.K. Wolff, T. Ziegler, E. van Lenthe, E.J. Baerends, J. Chem. Phys. 110 (1999) 7689.

[7] R. Fukuda, M. Hada, H. Nakatsuji, J. Chem. Phys. 118 (2003) 1015;
R. Fukuda, M. Hada, H. Nakatsuji, J. Chem. Phys. 118 (2003) 1027.

[8] M. Kaupp, V.G. Malkin, O.L. Malkina, D.R. Salahub, J. Am. Chem. Soc. 117 (1995) 1851;
M. Kaupp, V.G. Malkin, O.L. Malkina, D.R. Salahub, J. Am. Chem. Soc. 117 (1995) 8492;
M. Kaupp, V.G. Malkin, O.L. Malkina, D.R. Salahub, Chem. Phys. Lett. 235 (1995) 382.

[9] J. Vaara, O.L. Malkina, H. Stoll, V.G. Malkin, M. Kaupp, J. Chem. Phys. 114 (2001) 61.

[10] M. Kaupp, O.L. Malkina, V.G. Malkin, J. Chem. Phys. 106 (1997) 9201;
M. Kaupp, O.L. Malkina, J. Chem. Phys. 108 (1998) 3648;
M. Kaupp, V.G. Malkin, O.L. Malkina, D.R. Salahub, Chem. Eur. J. 2 (1996) 24;
M. Kaupp, Chem. Eur. J. 2 (1996) 348;
M. Kaupp, Chem. Ber. 129 (1996) 535.

[11] G. Schreckenbach, S.W. Wolf, T. Ziegler, J. Phys. Chem. A 104 (2000) 8244, and references therein.

[12] G. Schreckenbach, Inorg. Chem. 41 (2002) 6560.

[13] P. Schwerdtfeger, T. Fischer, M. Dolg, G. Igel-Mann, A. Nicklass, H. Stoll, A. Haaland, J. Chem. Phys. 102 (1995) 2051;
T. Leininger, A. Nicklass, H. Stoll, M. Dolg, P. Schwerdtfeger, J. Chem. Phys. 105 (1996) 1053.

[14] M. Straka, K.G. Dyall, P. Pyykkö, Theor. Chem. Acc. 106 (2001) 393.

[15] N. Ismail, J.-L. Heully, T. Saue, J.-P. Daudey, C.J. Marsden, Chem. Phys. Lett. 300 (1999) 296;
Y.-K. Han, K. Hirao, J. Chem. Phys. 113 (2000) 7345;
Y.-K. Han, J. Comput. Chem. 22 (2001) 2010.
[16] K.G. Dyall, Mol. Phys. 96 (1999) 511 (references therein).
[17] M. Straka, M. Patzschke, P. Pyykkö, Theor. Chem. Acc. 109 (2003) 332.
[18] M.J. Frisch, G.W. Trucks, H.B. Schlegel, G.E. Scuseria, M.A. Robb, J.R. Cheeseman, V.G. Zakrzewski, J.A. Montgomery, R.E.S. Jr., J.C. Burant, S. Dapprich, J.M. Millam, A.D. Daniels, K.N. Kudin, M.C. Strain, O. Farkas, J. Tomasi, V. Barone, M. Cossi, R. Cammi, B. Mennucci, C. Pomelli, C. Adamo, S. Clifford, J. Ochterski, G.A. Petersson, P.Y. Ayala, Q. Cui, K. Morokuma, D.K. Malick, A.D. Rabuck, K. Raghavachari, J.B. Foresman, J. Cioslowski, J.V. Oritz, A.G. Baboul, B.B. Stefanov, G. Lui, A. Liashenko, P. Piskorz, I. Komaromi, R. Gomperts, R.L. Martin, D.J. Fox, T. Keith, M.A. Al-Laham, C.Y. Peng, A. Nanayakkara, C. Gonzalez, M. Challacombe, P.M.W. Gill, B.G. Johnson, W. Chen, M.W. Wong, J.L. Andres, M. Head-Gordon, E.S. Replogle, J.A. Pople, Gaussian 98, Gaussian, Inc., Pittsburgh, PA, 1998.
[19] A.D. Becke, Phys. Rev. A 38 (1988) 3098.
[20] A.D. Becke, J. Chem. Phys. 98 (1993) 5648.
[21] A.D. Becke, J. Chem. Phys. 98 (1993) 1372.
[22] J.P. Perdew, Y. Wang, Phys. Rev. B 33 (1986) 8822.
[23] C. Lee, W. Yang, G.R. Parr, Phys. Rev. B 37 (1988) 785;
B. Miehlich, A. Savin, H. Stoll, H. Preuss, Chem. Phys. Lett. 157 (1989) 200.
[24] J.P. Perdew, in: P. Ziesche, H. Eschrig (Eds.), Electronic Structure of Solids '91, Akademie Verlag, Berlin, 1991.
[25] W. Küchle, M. Dolg, H. Stoll, H. Preuss, J. Chem. Phys. 100 (1994) 7535, Basis sets were obtained from the Extensible Computational Chemistry Environment Basis Set Database, Version 02/25/04, as developed and distributed by the Molecular Science Computing Facility, Environmental and Molecular Sciences Laboratory which is part of the Pacific Northwest Laboratory.
[26] P.J. Hay, R.L. Martin, J. Chem. Phys. 109 (1998) 3875.
[27] P.J. Hay, R.L. Martin, J. Chem. Phys. 109 (1998) 3875;
L. Gagliardi, B.O. Roos, Chem. Phys. Lett. 331 (2000) 229.
[28] T.H. Dunning Jr., J. Chem. Phys. 90 (1989) 1007;
R.A. Kendall, T.H. Dunning Jr., R.J. Harrison, J. Chem. Phys. 96 (1992) 6769.
[29] A. Schäfer, C. Huber, R.J. Ahlrichs, J. Chem. Phys. 100 (1994) 5829.
[30] B. Weinstock, G.L. Goodman, Adv. Chem. Phys. 9 (1969) 169.
[31] W. Kutzelnigg, U. Fleischer, M. Schindler (Eds.), The IGLO-Method: Ab Initio Calculation and Interpretation of NMR Chemical Shifts and Magnetic Susceptibilities, vol. 23, Springer-Verlag, Heidelberg, 1990.
[32] See, e.g.: R. Ditchfield, Mol. Phys. 27 (1974) 789;
K. Wolinski, J.F. Hinton, P. Pulay, J. Am. Chem. Soc. 112 (1980) 8251.
[33] C.J. Jameson, A.K. Jameson, J. Honarbakhsh, J. Chem. Phys. 81 (1984) 5266.
[34] V. Barone, M. Cossi, J. Phys. Chem. A 102 (1998) 1995;
S. Miertus, E. Scrocco, J. Tomasi, Chem. Phys. 55 (1981) 117;
R. Cammi, J. Tomasi, J. Comput. Chem. 16 (1995) 1449;
J. Tomasi, M. Persico, Chem. Rev. 94 (1995) 2027;
CPCM is based on the COSMO model: A. Klamt, G. Schüürman, J. Chem. Soc., Perkins Trans. 2 (1993) 799.
[35] A.E. Reed, F.J. Weinhold, Chem. Phys. 83 (1985) 1736;
A.E. Reed, L.A. Curtiss, F. Weinhold, Chem. Rev. 88 (1988) 899.
[36] G. Schreckenbach, Inorg. Chem. 39 (2000) 1265.
[37] H. Partridge, J. Chem. Phys. 90 (1989) 1043.
[38] M. Kaupp, O.L. Malkina, V.G. Malkin, P. Pyykkö, Chem. Eur. J. 4 (1998) 118.
[39] M. Straka, R. Reviakine, M. Kaupp (unpublished results).
[40] E.P. Zeer, O.V. Falaleev, V.E. Zobov, Chem. Phys. Lett. 100 (1983) 24.
[41] E.A Cuellar, T.J. Marks, Inorg. Chem. 20 (1981) 2129.
[42] S. Berger, S. Braun, H.-O. Kalinowski, NMR-Spektroskopie von Nichtmetallen, Georg Thieme Verlag, Stuttgart, 1994.
[43] A.V. Arbuznikov, M. Kaupp, Chem. Phys. Lett. 386 (2004) 8.
[44] W. Hieringer, F. Della Sala, A. Görling, Chem. Phys. Lett. 383 (2004) 115;
A.M. Teale, D.J. Tozer, Chem. Phys. Lett. 383 (2004) 109.
[45] V.G. Malkin, O.L. Malkina, R. Reviakine, A.V. Arbouznikov, M. Kaupp, B. Schimmelpfennig, I. Malkin, T. Helgaker, K. Ruud, MAG-ReSpect (Version1.1), 2003.
[46] See, e.g., chapter 18 in [3], and D. Auer, C. Strohmann, A.V. Arbuznikov, M. Kaupp, Organometallics 22 (2004) 2442.
[47] G. Schreckenbach, J. Chem. Phys. 110 (1999) 11936;
S. Patchkovskii, T. Ziegler, J. Chem. Phys. 111 (1999) 5730.